Searching for Gravitational Waves with a Geostationary Interferometer

Massimo Tinto,[*] J.C.N. de Araujo,[†] and Odylio D. Aguiar[‡]

Instituto Nacional de Pesquisas Espaciais,

Astrophysics Division Avenida dos Astronautas 1758,

12227-010 - São José dos Campos, SP, Brazil

Márcio Eduardo da Silva Alves[§]

Instituto de Ciências Exatas, Universidade

Federal de Itajubá, 37500-903 Itajubá, MG, Brazil

(Dated: August 3, 2012)

Abstract

We analyze the sensitivities of a geostationary gravitational wave interferometer mission operating in the sub-Hertz band. Because of its smaller armlength, our proposed Earth-orbiting detector will be less sensitive, by a factor of about seventy, than the Laser Interferometer Space Antenna (LISA) mission in the lower part of its accessible frequency band ($10^{-4} - 2 \times 10^{-2}$ Hz), while it will outperform it by the same factor in the higher-part of it ($2 \times 10^{-2} - 10$ Hz). By being able to probe the higher region of the sub-Hertz band with higher sensitivity, our proposed interferometer will observe a larger number of super-massive black holes (SMBHs) with masses smaller than $\sim 10^{6}$ $M_{\odot}$, thereby probing more accurately the astrophysical scenarios that account for their formation.

PACS numbers: 04.80.Nn, 95.55.Ym, 07.60.Ly

---

[*]Also at: Jet Propulsion Laboratory, California Institute of Technology, Pasadena, CA 91109

; Electronic address: Massimo.Tinto@gmail.com

[†]Electronic address: jcarlos.dearaujo@inpe.br

[‡]Electronic address: odylio.aguiar@inpe.br

[§]Electronic address: alvesmes@unifei.edu.br

I. INTRODUCTION

The quest for the direct observation of gravitational radiation is one of the most pressing challenges in the physics of this century. Predicted by Einstein shortly after formulating his general theory of relativity, gravitational waves (GW) will allow us to probe regions of space-time otherwise unobservable in the electromagnetic spectrum [1]. Although we have excellent indirect evidence of their existence through their effects on the orbital evolution of binary systems containing pulsars, we have not been able yet to directly detect them. Several ground-based gravitational wave detectors have been operational for awhile, and only recently they have been able to identify the most stringent upper limits to date for the amplitudes of the radiation expected from several classes of sources [2–5]. Next generation of Earth-based interferometers and pulsar-timing experiments [6], as well as newly conceived space-born detectors [7] are expected to achieve this goal.

Ground-based interferometers operate in the frequency band whose lower limit is at about 10 Hz, mainly because of the large seismic and gravity-gradient noises below this frequency cut-off. Since the mHz region is potentially very rich in gravitational wave sources, the most natural way to observe them is to build and operate a space-borne detector. The most notable example of a space interferometer, which has been under study for several years jointly by scientists in the United States of America and in Europe, is the Laser Interferometer Space Antenna (LISA) mission. By relying on coherent laser beams exchanged between three remote spacecraft forming a giant (almost) equilateral triangle, LISA aimed to detect and study cosmic gravitational waves in the $10^{-4} - 1$ Hz band.

Although over the years only a few space-based detector mission concepts have been considered as alternatives to the LISA mission (with ASTROD [8], DECIGO [9], and OMEGA [10]) being the most notable examples), starting in 2011 (with the ending of the NASA/ESA partnership for flying LISA) more missions concepts have appeared in the literature [11]. Their goals is to meet most (if not all) the LISA scientific objectives (highlighted in the 2010 Astrophysics Decadal Survey *New Worlds, New Horizons (NWNH)* [12], at a lower cost.

Given the present state of uncertainty about the future of this field in the United States and in Europe, and because the Brazilian Space Agency has expressed interest in pursuing the development and launch of several geostationary satellites, we have decided to analyze the scientific capabilities offered by a geostationary gravitational wave interferometer,

henceforth called GEOGRAWI[1].

GEOGRAWI, like LISA, has three identical spacecraft interchanging coherent laser beams and forming an (almost) equilateral triangle. However, by changing the spacecraft orbits from solar to geostationary, costs are reduced while a sensitivity complementary to that of LISA can be achieved in a frequency band that is starting just about one order of magnitude higher than that of LISA. It is worth noting that, although our interferometer reminds that of the OMEGA mission (proposed by R. Hellings [10] about 15 years ago), it is in fact very different from it. The OMEGA spacecraft were six in total, with two at each vertex of a geocentric equilateral triangle of side equal to one million kilometers. Cost of the launching vehicle as well as challenges in performing the phase measurements associated to the large relative velocities between the spacecraft make OMEGA quite different from GEOGRAWI.

The astrophysical sources that GEOGRAWI is expected to observe within its operational frequency band include extra-galactic massive and super-massive black-hole coalescing binaries, the resolved galactic binaries and extra-galactic coalescing binary systems containing white dwarfs and neutron stars, a stochastic background of astrophysical and cosmological origin, and possibly more exotic sources such as cosmic strings. With GEOGRAWI we will be able to test Einstein's theory of relativity by comparing the waveforms detected against those predicted by alternative relativistic theories of gravity, and also by measuring the number of independent polarizations of the detected gravitational wave signals [16].

Since the sensitivities of the geostationary interferometers we considered (see section II below) are degraded by their shorter armlength in the frequency region $(10^{-4} - 2 \times 10^{-2})$ Hz, it will be impossible for them to detect the zero-order cyclic spectrum of the white dwarf-white dwarf galactic binary confusion noise. However, as pointed out in [17], the periodic nature of the galactic background signal in the data of an interferometer rotating around the Sun will contain higher-order "cyclic spectra", which are in principle not affected by the instrumental noise (<u>if</u> this is stationary). This implies that we could still detect the so-called "confusion noise", and infer properties of the distribution of the white-dwarf binary systems present in our galaxy [17].

---

[1] We have recently discovered that Dr. Sean T. McWilliams, independently of us [13], has proposed a mission concept very similar to the one discussed in this paper [13, 14]. His concept and the one proposed by us, though strikingly similar, were nonetheless developed independently and submitted simultaneously to the recent NASA's Request for Information # NNH11ZDA019L [15]

In this article we pay particular attention to super-massive black holes, which are the main sources of GWs for interferometers operating at frequencies below 1 Hz. We show that GEOGRAWI will be able to detect a large number of SMBHs at very high redshifts, and that a significant fraction of them will have masses smaller than 10^6 M$_\odot$ as a consequence of its improved sensitivity at higher frequencies.

This paper is organized as follows. In section II we provide a description of the mission and a system noise analysis (mostly discussed in Appendix A) in order to evaluate the sensitivities of the Time-Delay Interferometric (TDI) [18] response X for three different on board subsystem configurations of GEOGRAWI, which we refer to as LISAGEO, Geostationary 1, and Geostationary 2. After noticing that the LISAGEO configuration (i.e. a LISA in a geostationary orbit) has a reduced sensitivity over that of LISA by a factor of about 70 in the lower part of its accessible frequency band ($10^{-4} - 2 \times 10^{-2}$ Hz), while it outperforms it by the same factor in the higher-part of it ($2 \times 10^{-2} - 10$ Hz), in section III we discuss possible sources of gravitational waves observable by GEOGRAWI and pay particular attention to SMBHs. Finally, in Section IV we provide a summary of our work and our conclusions.

II.   MISSION DESIGN AND INTERFEROMETER SENSITIVITIES

Our proposed space-based detector entails three spacecraft in geostationary orbit, forming an equilateral triangle with armlength of about $73,000$ km. Since the constellation plane coincides with the Earth equatorial plane, each spacecraft will need to be spherical and entirely covered with photo-voltaic cells. This will allow each spacecraft to be continuously powered (without the need of rotating it as the Earth orbits around the Sun) and maintain a high-level of thermal stability. It should be noticed also that the inclination (23.5^0) of the Earth equatorial plane with respect to the ecliptic will prevent (i) Sun light from contaminating the optics of the spacecraft during most of the interferometer orbital period around the Sun, and (ii) spacecraft occultation by the Earth. In proximity of the equinoxes, however, these properties will no longer be true and, in order to avoid these short-period operation interruptions, onboard electric power and Sun-light filters will need to be used. Sun-light filters needed for this purpose have already been developed for the OMEGA mission, which requires their usage at all times in its geocentric trajectory [19].

As the Sun and the Moon will exercise gravitational perturbations on each spacecraft

(resulting into a long-term orbital drift), in order to maintain orbital stability and small inter-spacecraft relative velocities, each spacecraft will need to implement "station-keeping" [20]. This is required not only for keeping the constellation in a stable configuration, but most importantly for relying on a phase-meter design that does not need to accommodate large relative frequency offsets, making it significantly less noisy (see appendix A). By taking the nominal value of 2 m/s/year for the "East-West" acceleration perturbation [20] acting on the spacecraft (which is responsible for the spacecraft relative velocities), it is easy to show that, in order to maintain their maximum velocities smaller than about a few decimeters per second, the station-keeping operation will need to be applied about once per week (see appendix A).

In order to estimate the TDI sensitivities of our geostationary GW interferometer detector, we have relied on some LISA study documents [7, 21]. This allowed us to derive a break-down estimate of the various noise sources affecting the TDI observables and compute the TDI sensitivities of a geostationary interferometer under the following three different on-board subsystem configurations:

(I) The onboard instrumentation is equivalent to that of the LISA mission. We will refer to this configuration as the "LISAGEO".

(II) The output power of the onboard lasers and the size of the optical telescopes are assumed to be equal to that of the LISA mission, while the noise performance of the accelerometers is taken to be a factor of ten worse than that of the accelerometers planned for the LISA mission. This configuration will be referred to as the "Geostationary 1". [2]

(III) The noise performance of each accelerometer is taken a factor of ten worse than that of the accelerometers planned for the LISA mission, the output power of the lasers is assumed to be a factor of 10 smaller than that of the lasers onboard LISA, and the diameter of the optical telescopes has been reduced by a factor of $\sqrt{10}$ over that of the LISA telescopes. This configuration will be called "Geostationary 2".

---

[2] This accelerometer noise level is equal to that of the accelerometer to be flown on-board the LISA Pathfinder mission [22, 23]
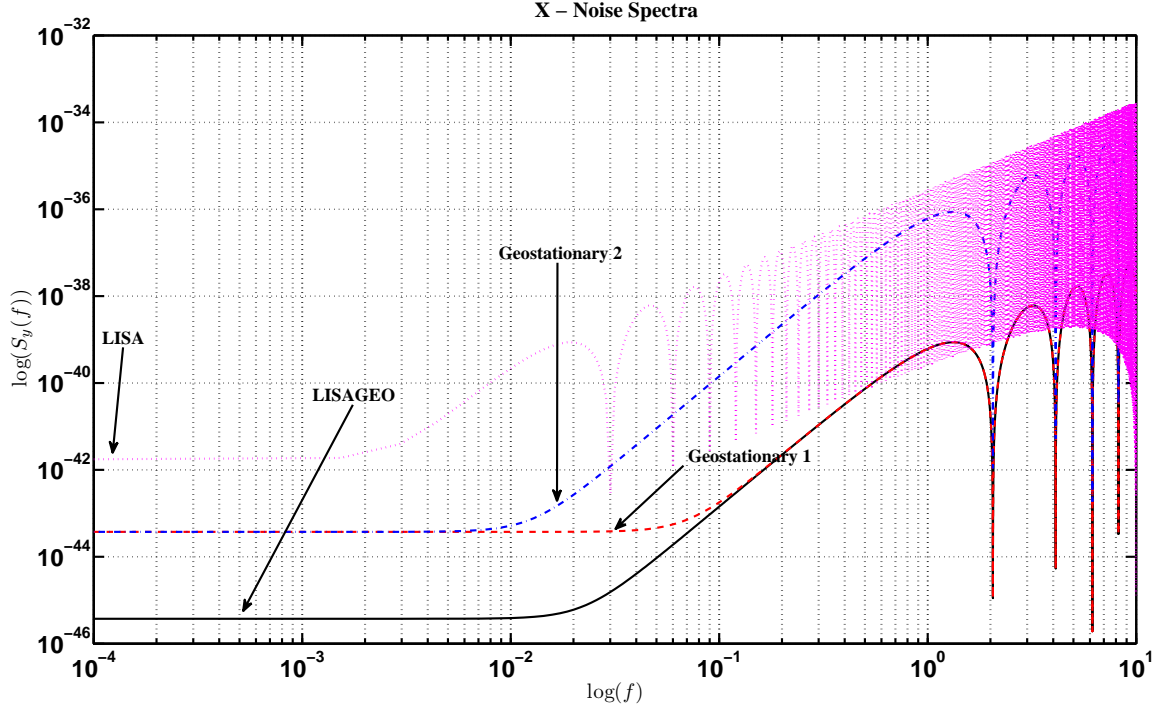
FIG. 1: Noise spectra for the X time-delay interferometric combination for the three on-board hardware configurations (I), (II), and (III) (see text). The varying depths of the minima in the high-frequency range is an artifact of numerically calculating these functions at discrete frequencies

The sensitivity of an interferometer detector of gravitational radiation has been traditionally taken to be equal to (on average over the sky and polarization states) the strength of a sinusoidal GW required to achieve a signal-to-noise ratio of 5 in a one-year integration time, as a function of Fourier frequency. For sake of simplicity we will limit the derivation of the sensitivities of the three geostationary configurations described above to only the "X" TDI combination, as those for the other TDI combinations can be inferred by properly scaling those for X. To this end we will be following the same procedure described in [24, 25], and rely on the following expression for the power spectrum of the noises affecting the X combination (see Figure 1)

$$S_X(f) = [8 \sin^2(4\pi f L) + 32 \sin^2(2\pi f L)]S_y^{pm}(f) + 16 \sin^2(2\pi f L) \, S_y^{op}(f) \qquad (1)$$

where $S_y^{pm}(f)$ is the spectrum of the relative frequency fluctuations due to each proof mass, and $S_y^{op}(f)$ is the spectrum of optical path (mainly shot and beam pointing) noise.

Both these noises have been regarded as the main limiting noise sources for LISA [7, 25], and can be treated as such for our geostationary interferometer configuration (see appendix A for details). The numerical expressions for the spectra $S_y^{pm}(f)$, $S_y^{op}(f)$ associated to the LISA mission were provided in [25] and they are equal to $S_y^{pm}(f)|_{LISA} = 2.5 \times 10^{-48} [f/1Hz]^{-2}$ Hz^{-1} and $S_y^{op}(f)|_{LISA} = 1.8 \times 10^{-37}[f/1Hz]^2$ Hz^{-1}. The configurations (I), (II) and (III) discussed above require appropriate scaling factors of these noise levels, and they are given in Table I (also see appendix A).

Mission	$S_y^{op}|_{LISA}$	$S_y^{pm}|_{LISA}$
LISA	1	1
LISAGEO	$(L_{GEO}/L_{LISA})^2$	1
Geo. 1	$(L_{GEO}/L_{LISA})^2$	10^2
Geo. 2	$(L_{GEO}/L_{LISA})^2 \times 10^3$	10^2

TABLE I: Noise spectra scaling factors as functions of the different instrument configurations analyzed. See text for more details.

Gravitational wave sensitivity is the wave amplitude required to achieve a given signal-to-noise ratio. We calculate it in the conventional way, requiring a signal-to-noise ratio of 5 in a one year integration time: $5 \sqrt{S_X(f) B}/$(root-mean-squared gravitational wave response of X). The bandwidth, B, was taken to be equal to one cycle/year (i.e. 3.17×10^{-8} Hz), while the root-mean-squared gravitational wave response was calculated by averaging over random sources of monochromatic GWs uniformly distributed over the celestial sphere and over their polarization states. This was done by taking the wave functions, $(h^{(+)}, h^{(\times)})$, in terms of a nominal wave amplitude, H, and the two Poincaré parameters, (Φ, Γ), in the following way [24]

$$h^{(+)}(t) = H \sin(\Gamma) \sin(\omega t + \Phi) , \tag{2}$$

$$h^{(\times)}(t) = H \cos(\Gamma) \sin(\omega t) . \tag{3}$$

We averaged over source direction by assuming uniform distribution of the sources over the celestial sphere, and also averaged over elliptical polarization states uniformly distributed on the Poincaré sphere for each source direction. The averaging was done via Monte Carlo
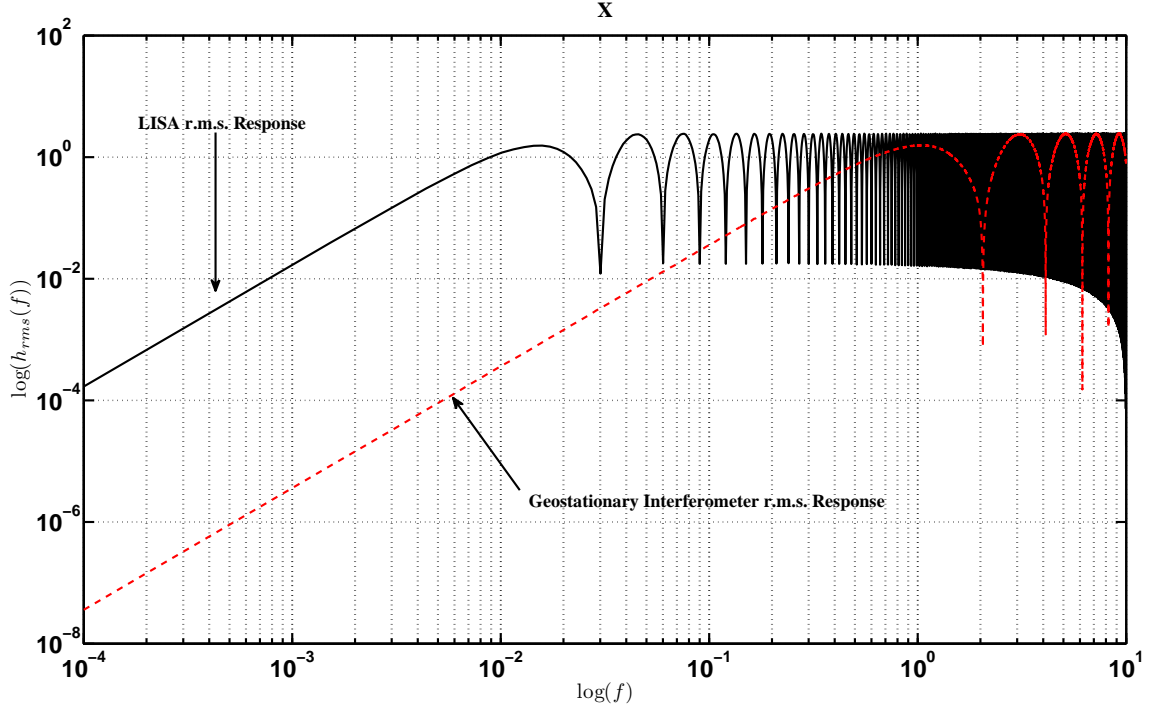
FIG. 2: Root-Mean-Square response of the X TDI combination for a geostationary interferometer. For completeness we have included also that for the interplanetary LISA mission, whose armlength is of 5×10^6 km. The r.m.s. has been calculated by assuming an ensemble of sinusoidal signals uniformly distributed on the celestial sphere and randomly polarized.

integration with 10000 source position/polarization state pairs per Fourier frequency bin and 10000 Fourier bins across the entire band analyzed $(10^{-4} - 10)$ Hz.

Figure (2) shows the root-mean-squared (r.m.s.) responses of the TDI combination X for a geostationary interferometer and for the interplanetary LISA mission (which is shown here for comparison). In the low-part of the accessible frequency band we may notice that the r.m.s. response of the geostationary interferometer is, as expected, penalized by the shorter armlength. At higher frequencies instead it is comparable to that of LISA because, in this region of the band, the response does no longer grow with the armlength of the detector. Note also that the varying depths of the minima in the high-frequency range is an artifact of numerically calculating these functions at discrete frequencies.

In Figure (3) we then plot the sensitivities of the TDI combination X for the various on-board hardware configurations discussed above. The characteristic behavior of the r.m.s.
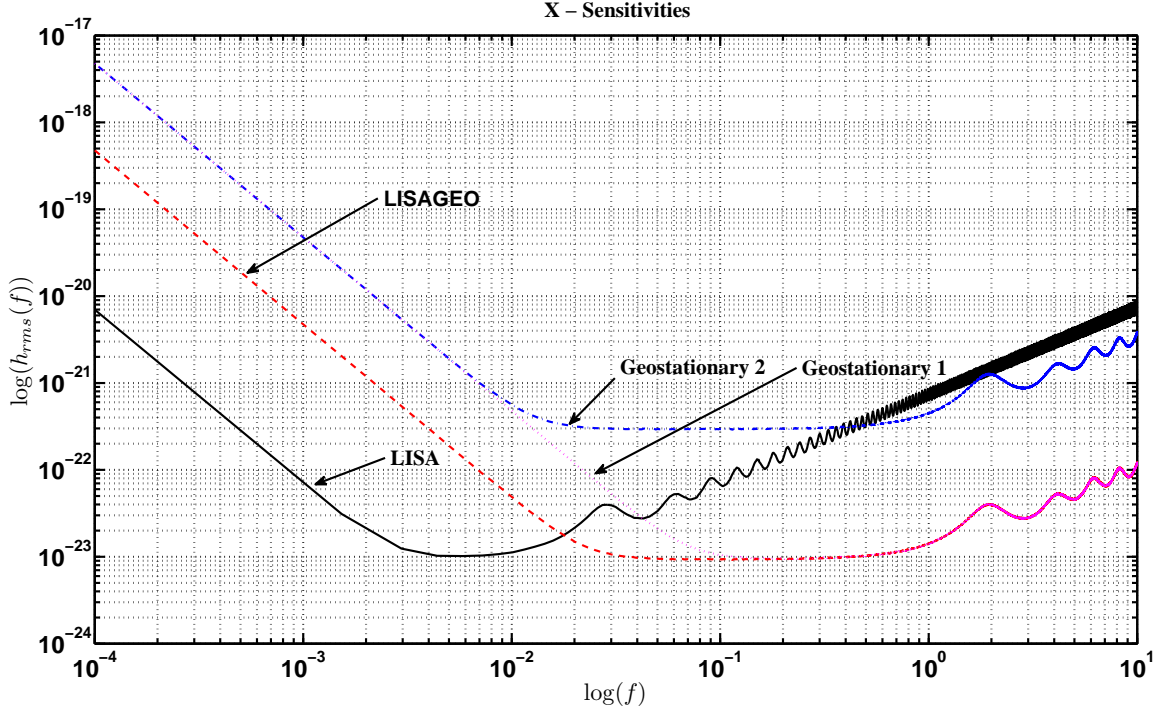
FIG. 3: Sensitivity of the X combination of a geostationary interferometer. Its noise performance is characterized by the noise spectra shown in Table (I) associated to the three different onboard subsystems configurations discussed. See text for more details.

responses in Figure (2) folds into the plots presented here. At high-frequencies the sensitivity of any of the geostationary interferometers considered is significantly better than that of the LISA mission while, at lower frequencies, the longer armlength of LISA results into a better sensitivity in this part of the band. Although the sensitivities at lower frequencies of any of the geostationary interferometers we considered are worse than that of the base-lined LISA mission (mostly because of the shorter armlength or worse accelerometer noise), they still will be able to provide a wealth of information about several astrophysical sources LISA was expected to detect and study. In the following section we turn to the science that a GEOGRAWI detector will be able to deliver.

9

III. SCIENCE WITH GEOGRAWI

In the previous section we have seen that a GEOGRAWI can operate in the $10^{-4} - 10$ Hz frequency band, and it could be more sensitive than LISA (configuration (I,II) discussed in section II) by a factor as large as 70 in the frequency region above 20 mHz. As a consequence of this result, it is natural to presume that a geostationary detector will be able to observe massive and super-massive Black Holes (SMBHs) and stellar-mass binary systems in the region of the frequency band where it achieves its best sensitivity. In the next subsections we focus our attention on SMBHs, as the sensitivity plots presented in Section II already imply the detectability of several binary systems present in our own galaxy (the so called "calibrators") [7], and other sources emitting in the higher region of the accessible frequency band.

A. Detecting Supermassive Black Holes with GEOGRAWI

A significant amount of GW energy can be released during the three evolutionary phases (namely inspiral, merger and ring-down) of coalescing binaries containing SMBHs (BSMBH). To assess how well and how often a geostationary interferometer could detect SMBHs during these three phases, we calculate below the maximum redshift, for a given signal-to-noise ratio (SNR), at which these systems could be detectable.

In order to perform this calculation we consider the formula for the SNR based on the matched filtering technique that relies on the waveforms discussed by Flanagan and Hughes [26] for characterizing the three evolutionary phases of the BSMBHs. The matched-filtering expression for the averaged squared SNR, in terms of the energy spectrum of the gravitational waves dE/df, is equal to [26]

$$\langle SNR^2 \rangle = \frac{2(1+z)^2}{5\pi^2 D_L(z)^2} \int_0^\infty df \, \frac{1}{f^2 S_h(f)} \frac{dE}{df}[(1+z)f] \, , \tag{4}$$

where z is the cosmological redshift of the source, D_L is the corresponding luminosity distance and $S_h(f)$ is the spectral density of the strain noise of the GW detector. In the left-hand-side of Eq. (4) the angle-brackets denote an ensemble average over sources uniformly distributed over the celestial sphere and polarizations.

Eq. (4) allows us to infer, for a given signal-to-noise ratio and a specific GEOGRAWI configuration, the maximum redshift at which a source can be detected, and then to estimate

the SMBHs observable event rate.

In the next subsections we separately consider the three different phases of the coalescing BSMBHs mentioned above. Our calculations are based on the analysis recently done by Filloux *et al.* [27, 28] on the formation and evolution of SMBHs.

1. Detecting SMBH in the Ringdown phase

In the present study the SMBHs are formed as a result of the merging of two other SMBHs, which for simplicity have been assumed with equal masses. The SMBH so formed goes through the process of "ringdown", and the resulting characteristic wave it emits is a damped sinusoid

$$h(t) \propto e^{-t/\tau} \cos(2\pi f_{rd}t) \ , \tag{5}$$

where τ is the characteristic ringdown damping time and f_{rd} is the frequency of the radiated signal. Following Ref. [26], the energy spectrum is equal to

$$\frac{dE}{df} \simeq \frac{1}{8}\mathcal{A}^2 Q M^2 f_{rd} \ \delta(f - f_{rd}), \tag{6}$$

where M is the SMBH mass, $\mathcal{A}$ is a dimensionless coefficient that describes the magnitude of the perturbation when the ringdown begins and Q is the quality factor of the mode.

Following Ref. [29], f_{rd} and Q can be related to the spin parameter a and to the mass M in the following way

$$f_{rd} \simeq \left[1 - 0.63(1 - a)^{3/10}\right] \frac{1}{2\pi M}, \tag{7}$$

$$Q = \pi \tau f_{rd} \simeq 2 \left(1 - a\right)^{-9/20} . \tag{8}$$

The energy associated with the ringdown process can be written as

$$E_{\rm rd} \simeq \frac{1}{8}\mathcal{A}^2 M^2 f_{rd} Q, \tag{9}$$

which we will take to be a fraction, ε_{rd}, of the total mass M of the black-hole. Although it has been argued in the literature that ε_{rd} could very well be as large as a few percents (see Ref. [26] for an interesting discussion on this issue), here we will consider only two different (conservative) values for it, namely: $\varepsilon_{rd} = 1 \ \%$ and $\varepsilon_{rd} = 0.1 \ \%$.

Finally, from the above equations the SNR can be rewritten in the following form

$$\langle SNR^2 \rangle = \frac{8}{5} \frac{\varepsilon_{rd}}{D_L(z)^2 F(a)^2} \frac{(1 + z)^3 M^3}{S_h[f_{rd}/(1 + z)]}, \tag{10}$$

11

where $F(a) = 1 - 0.63(1 - a)^{3/10}$.

With the expression (10) in hand we can calculate the redshift, z_{max}, below which a given SMBH of mass M can be detected with a specified SNR, spin parameter a and energy fraction ε_{rd}.

Since the luminosity distance depends on the cosmological parameters, in what follows we will assume a ΛCDM flat cosmology with the Hubble parameter $H_0 = 70 \, \mathrm{km \, s^{-1} \, Mpc^{-1}}$, the total matter density parameter $\Omega_M = 0.3$ and the cosmological constant density parameter $\Omega_\Lambda = 0.70$.

In Figure 4 we plot z_{max} as a function of the mass of the SMBH by taking SNR $= 10$ for the three GEOGRAWI configurations discussed in Section II. Also shown for comparison are the results for LISA with (LISA CN) and without (LISA) the confusion noise (CN) contribution. Since z_{max} mildly depends on the spin parameter a, we have fixed its value to 0.5. On the other hand, since z_{max} is very sensitive to the percentage of radiated energy, we have analyzed the following two possible values for ε_{rd}: 0.01 and 0.001.

Although LISA can observe these signals at much larger redshifts than any GEOGRAWI configuration discussed in this article, the LISAGEO configuration certainly represents an interesting alternative to LISA by being able to observe SMBHs at redshifts as high as $z = 10$ when $\varepsilon_{rd} = 0.01$. Moreover, LISAGEO is clearly more sensitive than LISA to SMBHs of masses $M < 10^6 \ M_\odot$ since they radiate at those frequencies for which LISAGEO is more sensitive than LISA.

From the above results we can now estimate the event rates of these systems for the different GEOGRAWI configurations. To perform this calculation we model the formation of SMBHs by relying on a recent study by Filloux et al. (see [27] and references therein), where the coalescence history of SMBHs is derived from cosmological simulations. Filloux et al. were able to derive the coalescence rate per unit volume and per mass interval as a function of the resulting BH mass and redshift (see Fig. 3 of [27]), $\Psi(M, z)$. With $\Psi(M, z)$ we can write the differential coalescence rate at the detector frame in the following way

$$dR_{obs}(M, z) = \frac{\Psi(M, z)}{1 + z} dM \frac{dV}{dz} dz \ , \tag{11}$$

where the factor $(1 + z)$ takes into account the time dilation.

For additional discussions, concerning the coalescence rate related to this study and the corresponding cosmological simulations, besides Ref. [27] we refer the reader to Ref. [28]
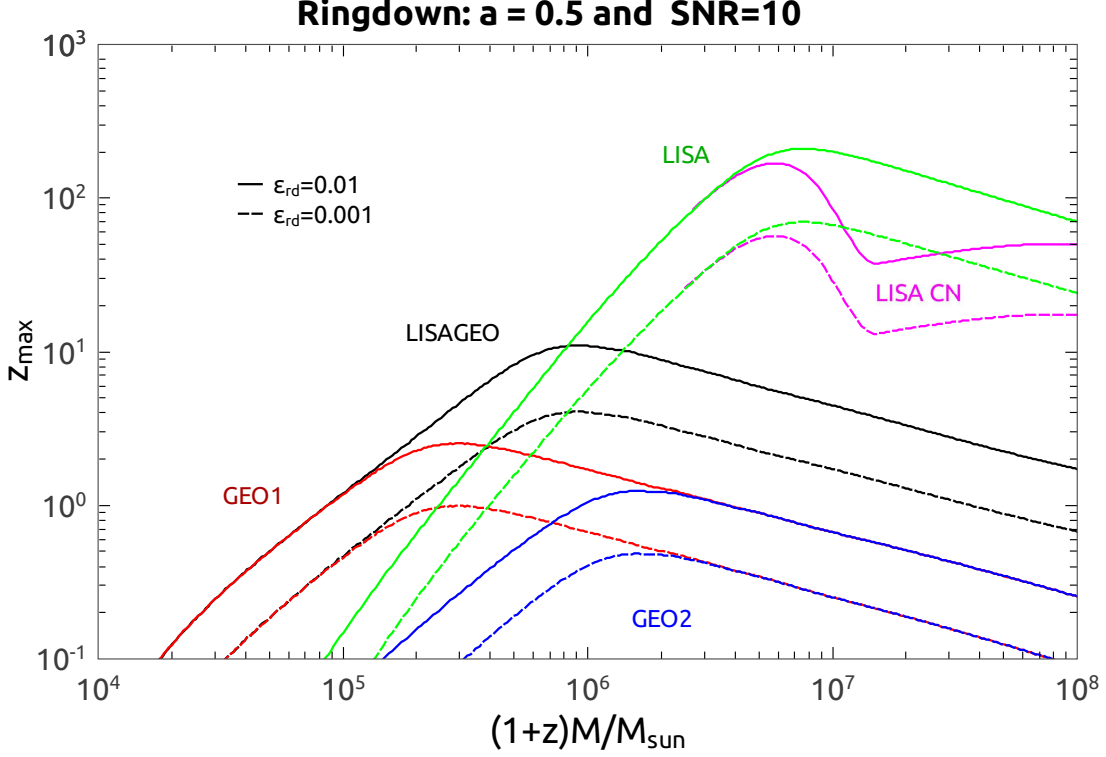
FIG. 4: z_{max} as a function of the SMBH mass M for $SNR = 10$, $a = 0.5$ and $\varepsilon_{rd} = 0.01$ and 0.001, for the three GEOGRAWI configurations. Also shown for comparison are the results for LISA with (LISA CN) and without (LISA) the confusion noise contribution.

and Appendix B.

Note that the above equation depends on the co-moving volume element dV which, for a flat cosmology, is equal to

$$dV = 4\pi \left(\frac{c}{H_0} \right) \frac{r^2(z)dz}{\sqrt{\Omega_\Lambda + \Omega_m(1+z)^3}} \tag{12}$$

and $r(z)$ is the co-moving distance

$$r(z) = \frac{c}{H_0} \int_0^z \frac{dz'}{\sqrt{\Omega_\Lambda + \Omega_m(1+z')^3}}. \tag{13}$$

With $z_{max}(M)$ we can now integrate Eq. (11) in the M and z variables to estimate the event rate for each GEOGRAWI configuration as a function of the SNR, a and ε_{rd}.

In Table II we show our estimated event rates for GEOGRAWI and, for comparison, also those for LISA. It can be noticed that, for $\varepsilon_{rd} = 0.01$, the event rates for LISAGEO are comparable to those for LISA. This can be better understood with the aid of Fig. 5, which
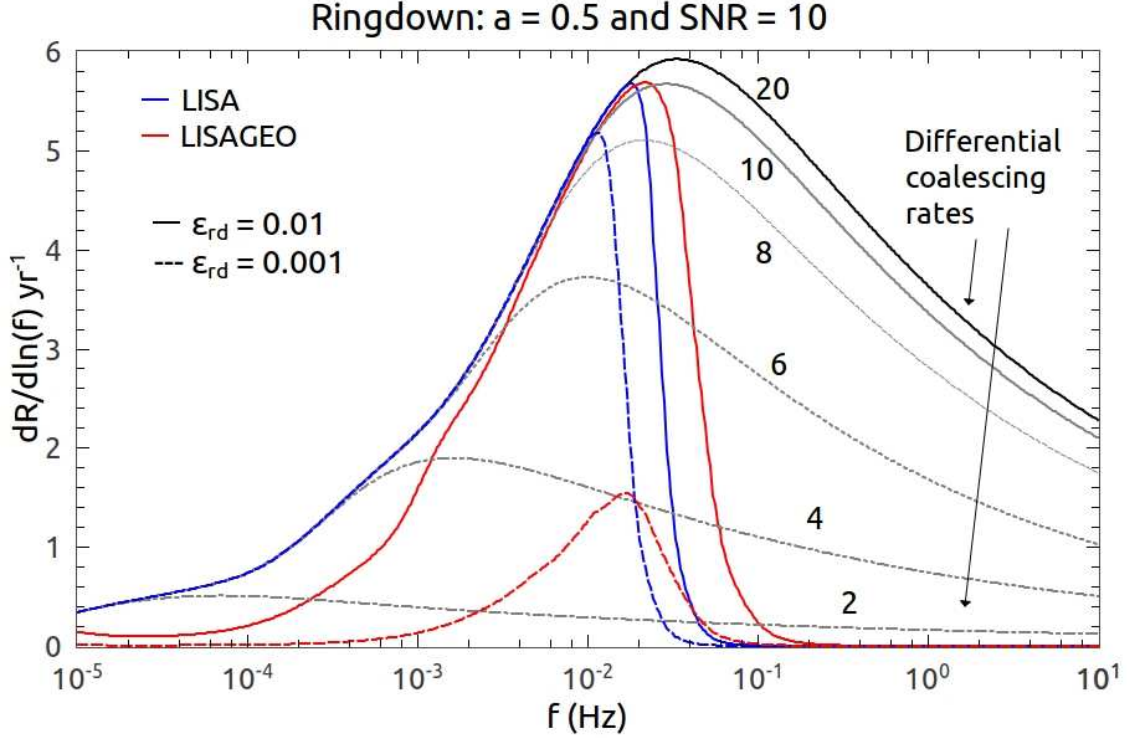
13

FIG. 5: Differential event rate as a function of frequency for the GEOGRAWI configuration 1 (LISAGEO) and for LISA. Also plotted, the differential coalescence rate for different redshift intervals; see Appendix B for details.

shows the logarithmic differential event rate as a function of frequency, together with the differential coalescing rate for comparison (see Appendix B for details.)

Note that when $\varepsilon_{rd} = 0.01$ the curve of the differential event rate of LISAGEO is above that of LISA at higher frequencies, where LISAGEO has a better sensitivity than LISA. In this region of its accessible frequency band LISAGEO can detect gravitational waves emitted by systems of smaller masses. Since these systems are larger in number than the more massive SMBHs, we can see why LISAGEO has an event rate comparable to that of LISA.

As shown in Appendix B, the model by Filloux et al. [27] for the current value of the coalescence rate amounts to $\simeq 43$ yr^{-1}. This implies that, depending on the values of ε_{rd} and a, LISAGEO can detect a large fraction of the SMBH coalescences.

TABLE II: The event rate for LISA, LISAGEO, GEO1 and GEO2 with a SNR $= 10$ and for different values of ε_{rd} and a.

Antenna	a	ε_{rd}	$R(\text{yr}^{-1})$
LISA CN	0	0.001	16.8
LISA CN	0.5	0.001	15.7
LISA CN	0.95	0.001	14.1
LISA CN	0	0.01	19.8
LISA CN	0.5	0.01	18.5
LISA CN	0.95	0.01	16.7
LISAGEO	0	0.001	2.41
LISAGEO	0.5	0.001	3.27
LISAGEO	0.95	0.001	5.29
LISAGEO	0	0.01	16.8
LISAGEO	0.5	0.01	18.3
LISAGEO	0.95	0.01	19.0
GEO1	0	0.001	0.049
GEO1	0.5	0.001	0.066
GEO1	0.95	0.001	0.10
GEO1	0	0.01	0.58
GEO1	0.5	0.01	0.82
GEO1	0.95	0.01	1.35
GEO2	0	0.001	0.008
GEO2	0.5	0.001	0.011
GEO2	0.95	0.001	0.018
GEO2	0	0.01	0.098
GEO2	0.5	0.01	0.13
GEO2	0.95	0.01	0.22

2. Detecting SMBH in the Merger phase

The merger phase can be related to a well defined Fourier frequency interval associated to the merger (lower) frequency f_m all the way to the radiation frequency f_{rd}. During this evolutionary phase a significant amount of GW energy, comparable to that emitted during the ring-down phase, is emitted.

The main issue regarding the characterization of the merger phase is the determination of the frequency f_m. We do not address this question here, and rely on the considerations made by Flanagan and Hughes [26], who take $f_m = 0.02/M$.

Following [26] we also assume the energy spectrum to be white and given by the following expression

$$\frac{dE}{df} = \frac{\varepsilon_m M}{f_{rd} - f_m}, \tag{14}$$

where ε_m is the fraction of the total mass M radiated during the merger phase. Here again we will analyze two cases corresponding to $\varepsilon_{rd} = 1\%$ and 0.1%. From the above equations the expression for the SNR can be written as follows

$$\langle SNR^2 \rangle = \frac{2(1+z)^2}{5\pi^2 D_L(z)^2} \frac{\varepsilon_m M}{f_{rd} - f_m} \int_{f_m/(1+z)}^{f_{rd}/(1+z)} \frac{df}{f^2 S_h(f)}. \tag{15}$$

Following the same prescription as for the ring-down case, we can then calculate the redshift, z_{max}, below which a given SMBH of mass M can be detected with a given SNR, spin parameter a and ε_{rd}. In Figure 6 we plot z_{max}, for the three different GEOGRAWI configurations, as a function of the mass M of the SMBH system for $SNR = 10$, $a = 0.5$ and $\varepsilon_m = 0.01$ and 0.001. As before we have included the results valid for LISA and LISA CN, and fixed the value of the spin parameter $a = 0.5$. Also in this case the LISAGEO configuration represents an interesting alternative to LISA as merging SMBHs could be seen at redshifts as high a $z = 10$ when $\varepsilon_{rd} = 0.01$.

3. Detecting SMBH in the inspiral phase

In this section we finally analyze the inspiraling phase of a binary system containing SMBH. In this case the signals frequency components will fall into the region of the band where $f < f_m$, which is accessible to all the GEOGRAWI configurations considered here.

The energy spectrum for the inspiraling phase is given by the well known formula [1]
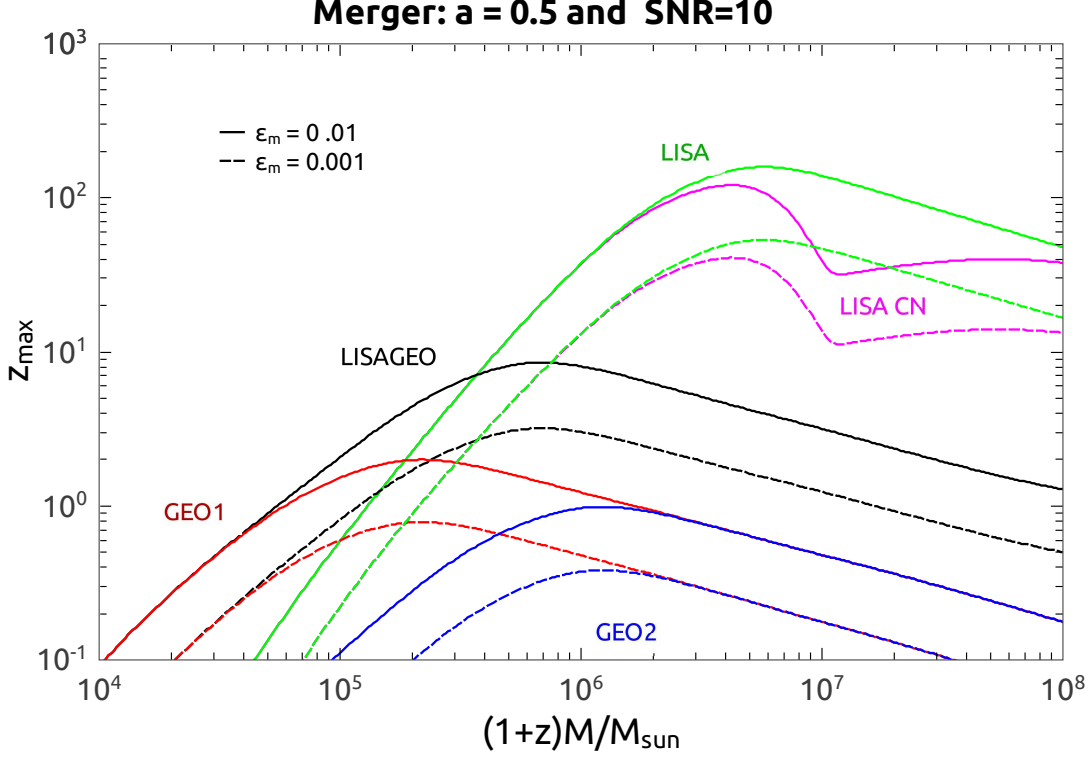
FIG. 6: z_{max} as a function of the SMBH mass M for $SNR = 10$, $a = 0.5$ and $\varepsilon_m = 0.01$ and 0.001, for the different GEOGRAWI configurations. Included for comparison are the results for LISA and LISA CN.

$$\frac{dE}{df} = \frac{1}{3}\pi^{2/3}\mu M^{2/3}f^{-1/3} \tag{16}$$

and, for the particular case of binary systems whose components have equal mass, the SNR becomes equal to

$$\langle SNR^2 \rangle = \frac{[(1+z)M]^{5/3}}{30\pi^{4/3}D_L(z)^2} \int_{f_{min}/(1+z)}^{f_m/(1+z)} \frac{df}{f^{7/3}S_h(f)}. \tag{17}$$

Note that now, in order to obtain z_{max} as a function of M, we had to treat the SNR and f_{min} as free parameters. As before, we take the $SNR = 10$. The value of f_{min} is chosen in such a way that the signal is integrated (observed) over the last year of inspiraling. For binary systems whose components have equal masses it is easy to show that f_{min} is given by the following expression

$$f_{min}(T) = \left\{ f_m^{-8/3} + \frac{64}{5}\pi^{8/3}[M(1+z)]^{5/3}T \right\}^{-3/8}, \tag{18}$$
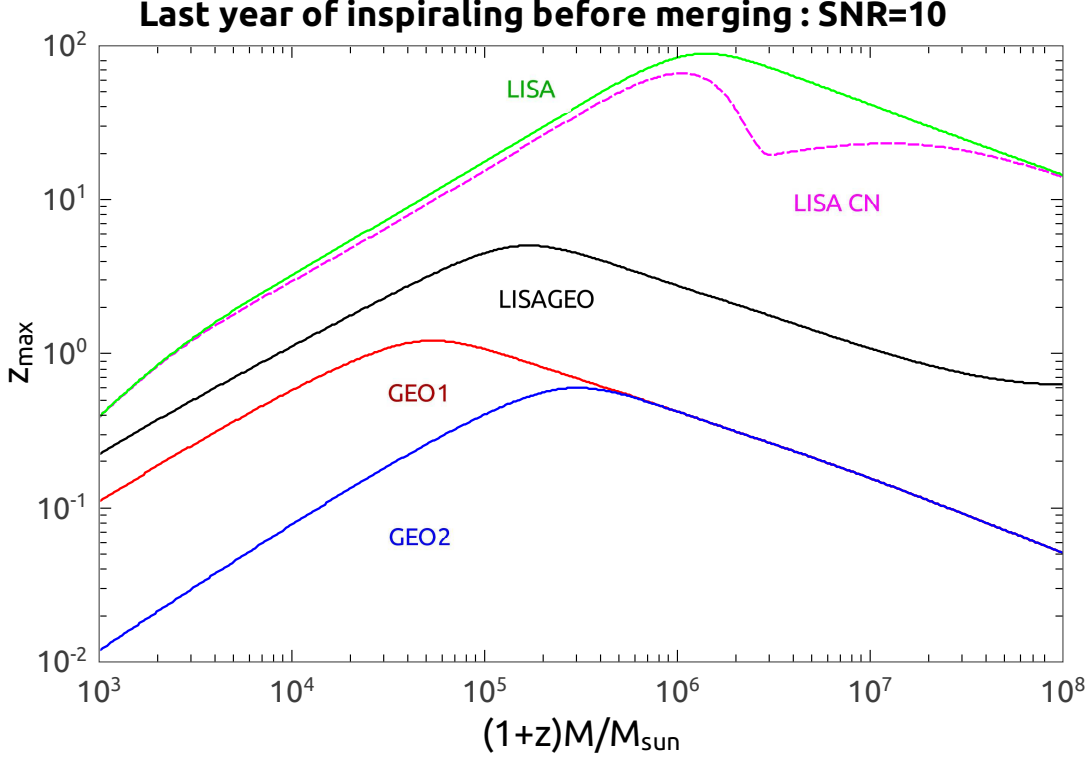
17

FIG. 7: z_{max} as a function of the SMBH mass M for $SNR = 10$ for the different LISA configurations. Also shown for comparison are the curves corresponding to LISA and LISA CN.

where T is the time before merging. In Figure 7 we plot z_{max} as a function of the mass of the system of SMBHs for SNR = 10 and for one year of observation.

Although Fig. (7) shows that a detection of the inspiral phase of the signal at an SNR=10 can be achieved by the LISAGEO configuration, it also indicates that the maximum redshift at which these signals can be seen is equal to about 5.

B. Pointing accuracies and parameters estimations

Although in our previous calculations of the SNR for the inspiral phase we have used an integration (observation) time of one year before merger, most of the contribution to the SNR comes from the last week or so before merger (see [7], page 116, where a similar consideration was made for LISA). During this time scale the GEOGRAWI antenna pattern is "scanned" several times during its daily revolutions around the Earth's rotation axis while that of LISA hardly changes. Since the GEOGRAWI amplitude modulation (which results into an observable frequency modulation) depends on the position of the SMBH binary

in the sky, and because GEOGRAWI achieves its best sensitivity level (equal to that of LISA) at higher frequencies, we conclude that LISAGEO should be able to reconstruct the SMBHs location in the sky and the other parameters that characterize it (masses, spin, distance, etc.) with accuracies better than those estimated for LISA. Although we plan to present in a forthcoming article a complete analysis of the so called "Inverse Problem for GEOGRAWI", from the above considerations it is possible to make an "educated guess" of the accuracies LISAGEO will achieve in reconstructing the SMBHs parameters by properly scaling those for LISA (see [7], page 113, section 4.4.3). From the sensitivity curves for LISA and LISAGEO and the accuracies estimated for the LISA mission [7] we can conservatively say that LISAGEO will be able to reconstruct the location of a SMBH binary system whose masses are in the range $10^4 - 10^6$ $M_\odot$ with an accuracy better than $10^{-5} - 10^{-3}$ steradians. The angular accuracies in the reconstructed source locations are somewhat larger than these for larger-mass SMBHs as they radiate at lower frequencies where LISAGEO is less sensitive, and also for smaller-mass BHs as their SNR are much smaller. The distance determination accuracy for SMBH mergers whose masses are in the $10^4 - 10^6$ $M_\odot$ range will be probably better than about 1% , while the determination of their masses can be expected to be better than $\Delta M/M = 0.1 - 1$ %.

IV. CONCLUSIONS

The main goal of this article was to analyze the performance and some scientific capabilities of a geostationary gravitational wave interferometer. We have done so by estimating its sensitivities to gravitational radiation when operated under three different onboard subsystem configurations, and analyzed the kind of gravitational wave sources it will be able to detect and study in the sub-Hertz band. We found our proposed Earth-orbiting detector less sensitive than the Laser Interferometer Space Antenna (LISA) mission by about a factor of seventy in the lower part of its accessible frequency band ($10^{-4} - 2 \times 10^{-2}$ Hz), while it outperforms it by the same factor in the higher-part of it ($2 \times 10^{-2} - 10$ Hz).

In the case of binary systems containing SMBHs, our analysis has shown the "LISAGEO" interferometer to be rather competitive to LISA in that it could observe a number of events per year comparable to that observable by LISA. This is because LISAGEO is more sensitive than LISA in the higher-frequency region of the accessible band, where lighter (and larger

in number) black-holes radiate in the ring-down phase.

Since most of the SNR from the coalescence phase of a binary system containing SMBHs is achieved after about a week of integration time before coalescence, because GEOGRAWI will be as sensitive as LISA in a higher part of the accessible frequency band, and because during a time period of one week the amplitude modulation of the GEOGRAWI response will result into a frequency modulation of the observed GW signal that depends on the source location in the sky, we have argued that the accuracies GEOGRAWI will achieve in the reconstructed GW source parameters will be better than those estimated for LISA in the case of SMBH masses that are in the range $10^4 - 10^6$ $M_\odot$. In a forthcoming article we will perform a more detailed analysis of the accuracies by which GEOGRAWI will be able to reconstruct the sky location of a SMBH binary and the parameters that characterize it (such as masses, distances, and spins). Since the high-part of the accessible frequency where GEOGRAWI achieves its best sensitivity is at around 1 Hz, we will investigate also its ability to perform low-latency searches of burst events. Jointly with its capability of continuously transmitting real-time data to the ground (by being geostationary), it should be able to trigger simultaneous searches for electromagnetic counter-parts.

Appendix A: Noise analysis

In this Appendix we provide an analysis of the noise sources affecting the heterodyne measurements performed by the geostationary GW interferometer "LISAGEO". Since its onboard instrumentation is similar to that of the LISA mission, it imposes the most stringent noise-performance requirements on the subsystems affecting the one-way heterodyne measurements.

Our analysis will rely on recent LISA study documents as guiding references [7, 21]. There

it was shown that there exist two main categories of sensitivity-limiting noise sources:

(I) Acceleration noises

(II) Optical-Path noises

The *acceleration noises* are due to residual forces acting on the proof-masses of the Gravitational Reduction System (GRS), and result into Doppler fluctuations into the heterodyne measurements. Their magnitudes are most prominent in the low-part of the accessible frequency band ($10^{-4} - 10^{-2}$ Hz) and depend on the (i) adopted GRS design, (ii) the spacecraft design, and (iii) the mission trajectory and space environment within which the spacecraft will be operating. For these reasons the classification of the acceleration noises is a multi-parameters problem and a very challenging one. In the case of the LISA mission this has already been studied extensively and it will be finalized through the LISA Pathfinder experiment [22, 23]. This is a ESA mission aimed at testing the noise modeling, classification, and performance of the LISA GRS system.

The LISA GRS was envisioned to have two cubic proof-masses onboard each spacecraft and whose positions relative to the spacecraft were measured with electrostatic (capacitative) readouts that were part of their caging systems. In recent years, however, it has been argued that a single, spherical proof-mass design (whose position relative to its enclosing cage is measured optically) could be used instead, providing significant simplifications of the GRS and of the optical bench where the heterodyne measurements are performed [30].

Although a single, spherical proof-mass GRS implementation might result into a better noise performance than that with two cubic masses [30], in our analysis we will assume LISAGEO to rely on a spherical GRS design whose performance is similar to that of the LISA GRS, i.e. with a square-root of the acceleration spectral density equal to a value of 3×10^{-15} m/s Hz$^{-1/2}$ over the accessible frequency band. In ultimate analysis it will be the LISA Pathfinder experiment that will show us whether the types and magnitudes of the noise sources affecting the GRS performance are what we expect them to be.

The primary noise sources within the second category, i.e. *Optical-path noises*, are much easier to identify and are most prominent in the higher part of the accessible frequency band. They can be summarized as [7, 21]

- Shot-noise at the photo-detectors,

- Residual laser phase noise in the TDI observables,

- Laser beam-pointing fluctuations,

- Phase-meter noise,

- Master clock noise,

- Scattered light effects.

The *Shot-Noise* is a fundamental noise limitation to the sensitivity of a laser interferometer GW detector in the high-part of its accessible frequency band. It affects the one-way Doppler measurements right at the photo-detector where two laser beams are made to interfere, and it leads to the following spectral density of relative frequency (Doppler) fluctuations [7]

$$S_{\text{shot}}(f) = \frac{h f^2}{\nu_0 \ P_{\text{avail}}} \ . \tag{A1}$$

In Eq. (A1) h is the Planck constant, $\nu_0 \equiv 3.0 \times 10^{14}$Hz is the nominal laser frequency, f is the Fourier frequency, and P_{avail} is the effective power available at the receiving photodetector. By assuming the same optics, optical telescope size, laser power, and photodetector quantum efficiency as those of LISA, from Eq. (A1) we conclude that the amplitude of the relative frequency fluctuations due to shot noise affecting the LISAGEO interferometer scale down linearly with the interferometer armlength.

The *Residual laser phase noise* represents the "left-over" of the laser noise in the TDI observables after the TDI algorithm is applied to the one-way Doppler measurements by properly time-shifting and linearly combining them. It is primarily due to the finiteness in the accuracy by which the armlengths are known, and is proportional to the amplitude of the laser frequency fluctuations. The relationship between the magnitude of the spectrum of the residual laser frequency fluctuations, $S_{\Delta C}(f)$, and the armlength accuracies, $\delta L_i \ , i = 1, 2$, is given in [31] for the unequal-arm Michelson interferometer TDI combination and has the following form

$$
\begin{aligned}
S_{\Delta C}(f) \ = \ & 64\pi^2 f^2 S_C(f) \left\{ \delta L_1^2 \sin^2(2\pi f L_2) + \delta L_2^2 \sin^2(2\pi f L_1) \right. \\
& \left. - \ \delta L_1 \delta L_2 [\sin^2(2\pi f L_1) + \sin^2(2\pi f L_2) - \sin^2(2\pi f (L_2 - L_1))] \right\} \ .
\end{aligned} \tag{A2}
$$

In the long-wavelength limit it is easy to show from the above equation that the amplitude of the residual laser frequency fluctuations scale linearly with the armlength of the

interferometer (see Eq. (3.18) of [31]). On the other hand, this scaling no longer exists at higher-frequencies and, in order to maintain this noise source negligible in the LISAGEO noise budget, a higher level of accuracy in the knowledge of the armlengths is required. Since the LISAGEO configuration will have a shot noise amplitude smaller than that of LISA by about a factor of 70, by measuring the LISAGEO armlength with an accuracy that is seventy times better than that of LISA we will make this noise source negligible in the LISAGEO TDI combination X. Given that the required LISA armlength accuracy for X has been estimated to be equal to about 30 meters [31], we conclude that the armlength accuracy needed for LISAGEO should be of about 40 centimeters. Such a level of laser ranging accuracy has already been demonstrated experimentally [32] at a much lower receiving laser power. This means that, in the case of the LISAGEO mission, the achievable armlength accuracy will be smaller than 40 cm, further reducing the LISAGEO residual laser frequency noise.

The *Laser beam-pointing fluctuations* are due to distortions in the transmitted laser beam wavefront that appear at the receiving spacecraft as additional frequency fluctuations generated by small pointing fluctuations from the transmitting spacecraft. In the case of the LISA mission, whose pointing fluctuations specifications were required not to be greater than 6 nrad $Hz^{-1/2}$, it was shown [33] that a way for substantially reducing pointing-induced frequency fluctuations was to rely on the light received from the far spacecraft to sense the orientation of the receiving spacecraft. An ingenious way for doing so [33] is by sampling some of the incoming light on a CCD array. By detecting the position of the beam on the CCD it is then possible to deduce the alignment of the spacecraft and implement it by proper control signals. This measurement is shot-noise limited and, in the case of the LISA mission, it was proposed to implement it by extracting 10 percent of the power of the incoming laser light. This resulted into a pointing noise of about 0.5 nrad $Hz^{-1/2}$, more than a factor of 10 better than that specified for LISA. Since the shot-noise level associated with this pointing measurement technique scales down linearly with the armlength (by being inversely proportional to the square-root of the received laser power) we conclude that the pointing shot-noise limit for LISAGEO will scale down linearly with the armlength from the level estimated for LISA.

The *Phase-meter* is the subsystem that measures the difference between the phase of the incoming laser beam and that from the local laser, and in the process it introduces an additional phase noise in the one-way Doppler measurements. Although the noise it

generates does not scale with the armlength, it does depend on the magnitude of the relative frequency offset between the transmitted and received frequencies of the two interfering laser beams [34]. As an example, it has been shown that the frequency stability of the phase-meter to be flown on the LISA Pathfinder mission (which has an heterodyne frequency range of about a few kHz) will be several orders of magnitude better than that of the phase-meter for the LISA mission [34, 35]. It is for this reason that, in order to compensate for the Sun and the Moon gravitational perturbations on each spacecraft and maintain orbital stability and small inter-spacecraft relative velocities, each spacecraft will implement "station-keeping" [20, 36]. Since this operation will need to be performed about once per week [37] in order to maintain the spacecraft relative velocities smaller than about a few decimeters per second, it will not disrupt significantly the science data acquisition. As an additional note, LISAGEO will also rely on molecular iodine laser frequency stabilization, which has been shown to provide laser frequency stability superior to that achievable by optical cavity stabilization and a laser frequency accuracy at the level of 1 to 2 kHz [38].

The *Master clock noise* affects the LISA measurements because it is used for removing the large Doppler beat-notes (as large as 20 MHz) affecting the Doppler measurements. Since LISAGEO will not be subject to large orbital perturbations as those affecting LISA and it will rely on station-keeping in order to maintain a "stationary" configuration, the noise due to the onboard master clock for performing the heterodyne measurements will be negligible as it is proportional to the magnitude of the beat note at the photodetector [39]. This will result into a significant simplification of the designs of the phase-meter and transmitting modules as modulations of the transmitting and receiving beam (for implementing the clock-noise cancellation scheme) will not be needed.

Scattered Light effects are due to spurious light signals generated from the interaction of the received main laser beam with the optical telescope, beam-splitter, and other optical components the beam interacts with before being made to interfere with the light of the local laser. Although this noise source has been thought for quite sometimes to be unavoidable, in recent years new developments in laser metrology have indicated that scattered light noise can be suppressed to sub-picometer levels in the frequency band of interest to space-based GW interferometers. In one such laser metrology technique, called "Digital Interferometry" (DI) [40, 41], laser light is phase modulated with a pseudo-random noise (PRN) code that time stamps the light, allowing isolation of individual propagation paths based on their

times of flight through the system. After detection, the PRN phase shift is removed by decoding with an appropriately delayed copy of the code. By matching the decoding delay to the propagation delay the signal is coherently recovered, allowing phase measurements to extract displacement information at resolutions much smaller than the laser wavelength. This matched-delay filtering of DI allows isolation of reflections from an object at a particular distance, such as the optical components giving origin to the scattered light noise.

In summary, the magnitude of the relative frequency fluctuations due to the shot-noise and the laser beam-pointing fluctuations scale linearly with the armlength, as it follows from the considerations leading to equation (4.4) at page 82 of [7], and sections 3 at page 1576 of [33] respectively. Although the frequency fluctuations due to the residual laser phase noise, the scattered-light noise, and the phase-meter noise do not follow a similar scaling, we have shown that they can be made negligible within the LISAGEO noise budget. This is because of a demonstrated better armlength accuracy [32], of digital interferometry as it suppresses scattered light effects, and adoption of a simpler phase-meter design [34] that takes advantage of much smaller "beat-note" frequencies among the lasers. The latter is made possible through a combination of laser iodine stabilization [38] together with spacecraft station-keeping maneuvers [20].

Appendix B: Coalescence rate

In this appendix we discuss the differential coalescence rate per logarithm frequency interval as this can be related to the differential event rate associated, for example, with the ring-down phase shown in Fig. 5. For a more detailed analysis regarding the coalescence rate and the corresponding cosmological simulations, we refer the reader to Refs. [27] and [28] respectively.

The differential coalescence rate is obtained from an appropriate combination of Eqs. (11) and (7) and an integration in a given redshift interval, namely $0 < z < z_{initial}$, where $z_{initial}$ refers to a value selected at the beginning of the simulation.

Fig. 8 shows the differential coalescence rate per logarithmic frequency interval as a function of the frequency and for different intervals of integration in the redshift. We have not included curves corresponding to values of the redshift higher than 20 because they all "saturate" to the curve corresponding to this value of $z_{initial}$.
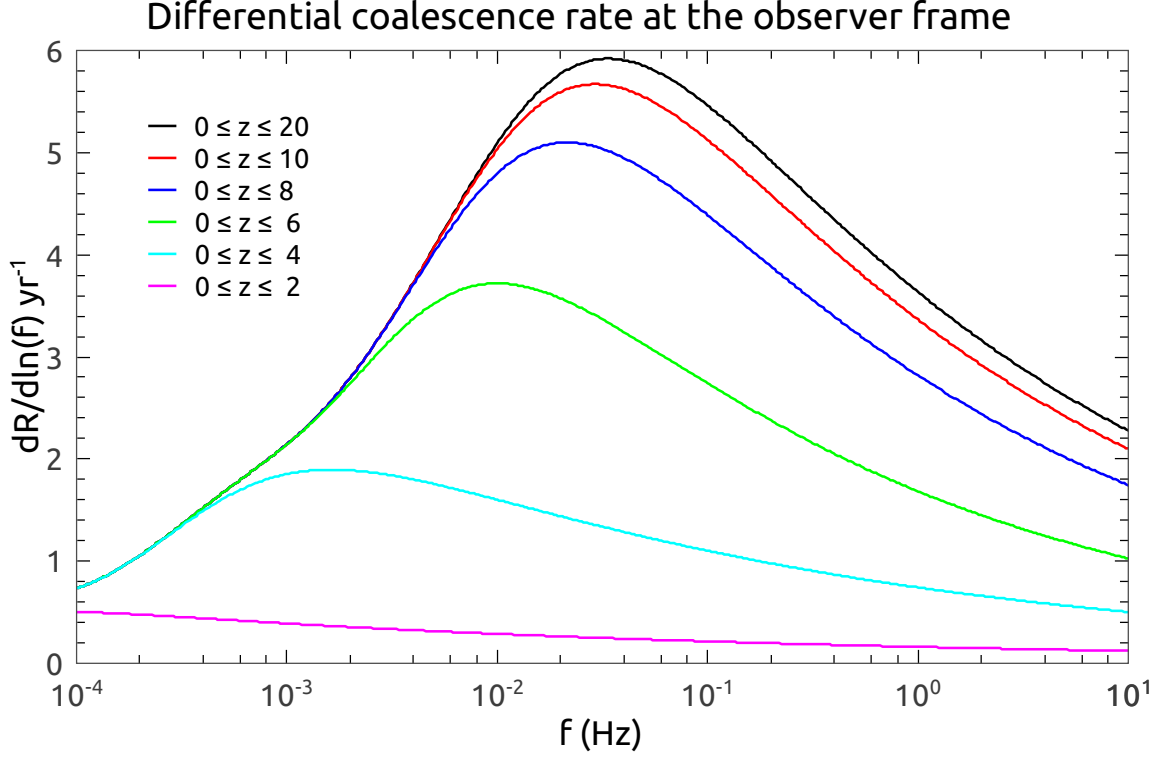
FIG. 8: Differential coalescence rate as a function of the Fourier frequency and for different interval of integration in redshift.

Another interesting information concerning the study by Filloux et al. [27] refers to the coalescence rate at the observer frame, which can be obtained by integrating the differential coalescence rate. After performing such an integration we find a coalescence rate of $\sim 43 \text{ yr}^{-1}$, which should be regarded as the maximum event rate a given gravitational wave antenna might detect. Our study has actually shown that LISA and LISAGEO should be able to detect a large fraction of this rate.

Implicit in the integration just mentioned, there is an integration in the redshift interval $0 < z < z_{initial}$, where $z_{initial}$ was taken to be equal to 60 in the present study. In practice, however, there is a saturation around $z \sim 12$, as can be seen in Fig. 9, where the cumulative event rate as a function of $z_{initial}$ is plotted and tabulated. Note that half of the coalescence rate comes from events occurring at $z > 5$.
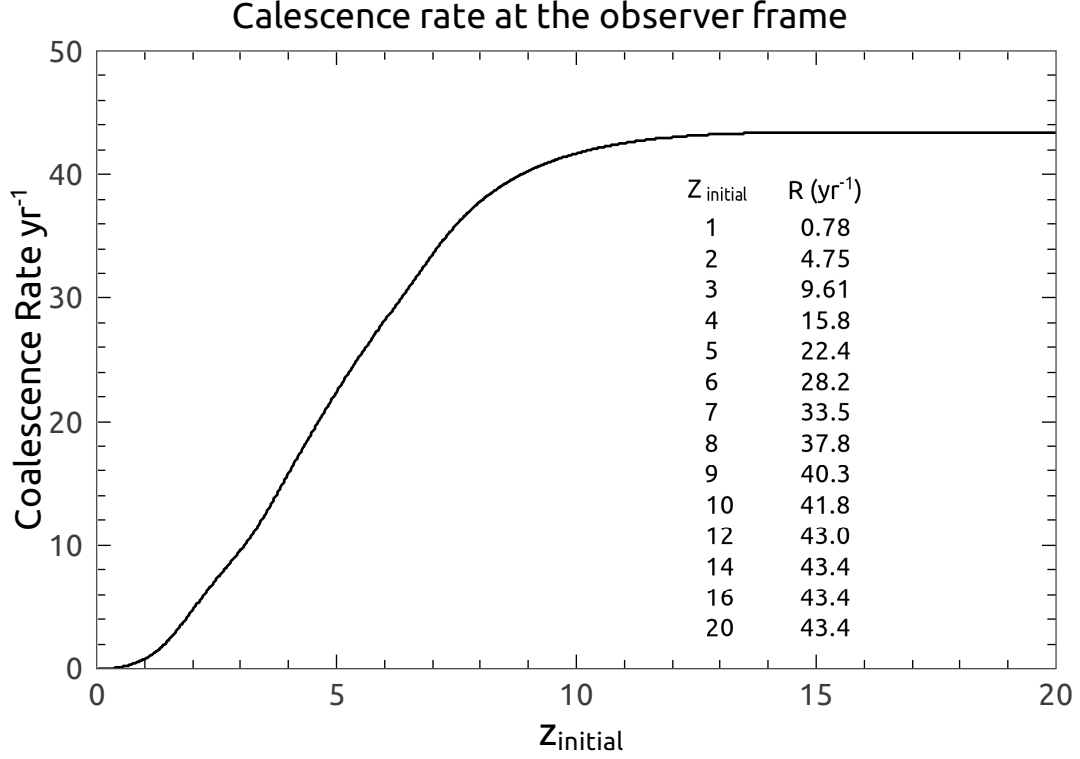
Calescence rate at the observer frame

$Z_{initial}$	R (yr^{-1})
1	0.78
2	4.75
3	9.61
4	15.8
5	22.4
6	28.2
7	33.5
8	37.8
9	40.3
10	41.8
12	43.0
14	43.4
16	43.4
20	43.4

FIG. 9: Coalescence rate as a function of $z_{initial}$. Note how this function starts to plateau at $z_{initial} \approx 12$.

[1] K.S. Thorne. In: *Three Hundred Years of Gravitation*, 330-458, Eds. S.W. Hawking, and W. Israel (Cambridge University Press: New York), (1987).

[2] http://www.ligo.caltech.edu/ .

[3] http://www.virgo.infn.it/ .

[4] http://www.geo600.uni-hannover.de/ .

[5] http://tamago.mtk.nao.ac.jp/ .

[6] S. Detweiler, *Ap. J.,* **234**, 1100-1104 (1979).

[7] P. Bender, K. Danzmann, & the LISA Study Team, Laser Interferometer Space Antenna for the Detection of Gravitational Waves, Pre-Phase A Report, MPQ233 (Max-Planck- Institüt für Quantenoptik, Garching), July 1998.

[8] W. T. Ni, *Int. J. Mod. Phys. D*, **11** (7), 947 (2002).

[9] N. Seto, S. Kawamura, and T. Nakamura, *Phys. Rev. Lett*, **87**, 221103 (2001).

[10] B. Hiscock, R.W. Hellings, *Bull. Am. Astron. Soc.*, **29**, 1312, (1997).

[11] http://pcos.gsfc.nasa.gov/studies/gravitational-wave-mission.php/ .

[12] NRC 2010, http:// www.nap.edu/catalog/12951.html

[13] M. Tinto, J.C.N. de Araujo, O.D. Aguiar, and M.E.S. Alves, *A Geostationary Gravitational Wave Interferometer (GEOGRAWI)* (http://arxiv.org/pdf/1111.2576.pdf).

[14] S.T. McWilliams, *Geostationary Antenna for Disturbance-Free Laser Interferometry (GAD-FLI)* (http://arxiv.org/PS_cache/arxiv/pdf/1111/1111.3708v1.pdf).

[15] NASA solicitation # NNH11ZDA019L titled: *Concepts for the NASA Gravitational-Wave Mission*. Document available at: http://nspires.nasaprs.com/external/ .

[16] M. Tinto and M.E.S. Alves, *Phys. Rev. D,* **82**, 122003 (2010)

[17] J.A. Edlund, M. Tinto, A. Królak, G. Nelemans, *Classic. Quantum Grav.*, **22**, S913-S926 (2005)

[18] M. Tinto and S.V. Dhurandhar, *Living Rev. Relativity*, **8**, 4, (2005). http://www.livingreviews.org/lrr-2005-4

[19] R. Hellings, S.L. Larson, S. Jensen, C. Fish, M. Benacquista, N. Cornish, and R. Lang, *A LOW-COST, HIGH-PERFORMANCE SPACE GRAVITATIONAL ASTRONOMY MISSION* (http://pcos.gsfc.nasa.gov/studies/rfi/GWRFI-0007-Hellings.pdf).

[20] E. M. Soop, *Handbook of Geostationary Orbits*, Kluwer Academic Publishers, Dordrecht, (1994).

[21] "LISA: Unveiling a hidden Universe", ESA publication # ESA/SRE(2011)3 (February 2011). Also available at: http://sci.esa.int/science-e/www/object/index.cfm?fobjectid=48364

[22] F. Antonucci *et al*, *Class. Quantum Grav.,* **28** 094001, (2011).

[23] F. Antonucci *et al*, *Class. Quantum Grav.,* **28** 094002, (2011).

[24] J.W. Armstrong, F.B. Estabrook and M. Tinto, *Ap. J.,* **527**, 814 (1999).

[25] F.B. Estabrook, M. Tinto, and J.W. Armstrong, *Phys. Rev. D,* **62**, 042002 (2000).

[26] E.E. Flanagan and S.A. Hughes, *Phys. Rev. D,* **57**, 4535 (1998)

[27] Ch. Filloux, J.A. de Freitas Pacheco, F. Durier and J.C.N. de Araujo, *IJMPD*, **20**, 2399 (2011); arXiv:1108.2638

[28] Ch. Filloux, F. Durier, J.A. de Freitas Pacheco and J. Silk, *IJMPD*, **19**, 1233 (2010).

[29] F. Echeverria, *Phys.Rev. D* **40**, 3194 (1989).

[30] Ke-Xun Sun, G. Allen, S. Buchman, D. DeBra and R. Byer, *Class. Quantum Grav.,* **22**, S287

- S296, (2005).

[31] M. Tinto and J.W. Armstrong, *Phys. Rev. D,* **59**, 102003 (1999).

[32] J.J. Esteban, A.F. Garcia, S. Barke, A.M. Peinado, F.G. Cervantes, I. Bykov, G. Heinzel, and K. Danzmann, *Opt. Express*, **19**, 15937, (2011).

[33] D.I. Robertson, P. McNamara, H. Ward and J. Hough, *Class. Quantum Grav.,* **14**, 1575 (1997).

[34] V. Wand, *Interferometry at low frequencies: optical phase measurement for LISA and LISA Pathfinder*, Ph. D. thesis, University of Hannover, unpublished (2007).

[35] D. Shaddock, B. Ware, P. Halverson, R.E. Spero and B. Klipstein, *Overview of the LISA Phasemeter*, International LISA Symposium 2006, eds. S.M. Merkowitz, and J.C. Livas, Springer, Berlin, Germnay, pp. 654-660 (2006).

[36] G. Maral and M. Bousquet, *Satellite Communications Systems*, fifth edition, John Wiley & Sons, Chichester, England, U.K. (2009).

[37] A.A. Kamel, W. Gelon, and K. Reckdahl. In proceedings of: *AAS/AIAA Astrodynamics Specialist Conference*, Girdwood, Alaska, August 16-18, 1999, AAS Paper No. AAS 99-388.

[38] V. Leonhardt, and J.B. Camp, *APPLIED OPTICS*, **45**, 4142 (2006).

[39] M. Tinto, F.B. Estabrook, and J.A. Armstrong, *Phys. Rev. D,* **65**, 082003 (2002).

[40] D. A. Shaddock, *Opt. Lett.*, **32**, 3355 (2007).

[41] D. M. R. Wuchenich, T. T.-Y. Lam, J. H. Chow, D. E. McClelland, and D. A. Shaddock, *Opt. Lett.*, **36**, 672 (2011).